





INVITED PAPER

Caudal Spine Morphology and Puncture Performance of Two Coastal Stingrays

Caitlin S. Shea-Vantine,* Katherine A. Galloway *[†] Danielle N. Ingle,*[‡]
Marianne E. Porter * and Stephen M. Kajiura*¹

*Department of Biological Sciences, Florida Atlantic University, Boca Raton, FL 33431, USA; [†]Department of Biological Sciences, Nicholls State University, Thibodaux, LA 70310, USA; [‡]Department of Marine Biology, Texas A&M University at Galveston, Galveston, TX 77554, USA

¹E-mail: kajiura@fau.edu

Synopsis A diagnostic characteristic of stingrays in the family Dasyatidae is the presence of a defensive, partially serrated spine located on the tail. We assessed the contribution of caudal spine morphology on puncture and withdrawal performance from two congeneric, co-occurring stingrays, the Atlantic stingray, *Hypanus sabinus*, and the bluntnose stingray, *Hypanus say*. Spines exhibited a high degree of morphological variability. Stingray spines were serrated along 50.8% (*H. sabinus*) or 62.3% (*H. say*) of their length. *Hypanus say* had a greater number of serrations along each side of the spine (30.4) compared with *H. sabinus* (20.7) but the pitch did not differ between species. We quantified spine puncture and withdrawal forces using porcine skin as a model for human skin. Puncture and withdrawal forces did not differ significantly between species, or within *H. say*, but withdrawal force was greater than puncture force for *H. sabinus*. We incorporated micro-computed tomography scanning to quantify tissue mineral density and found that for both species, the shaft of the spine was more heavily mineralized than the base, and midway (50%) along the length of the spine was more heavily mineralized than the tip. The mineralization variability along the spine shaft may create a stiff structure that can fracture once embedded within the target tissue and act as an effective predator deterrent.

Introduction

Stingrays are named for their caudal spine, also referred to as a caudal barb or stinger. The spine is dorsoventrally compressed with a sharp, pointed tip, and with lateral, rear-facing serrations (with respect to the tip) on both sides (Fig. 1). The spine is positioned on the dorsal surface of the tail from near the base to near the tip, depending on the species (Su et al. 2017; Hughes et al. 2018). Spines first appeared on myliobatid stingrays from the Late Cretaceous period, which corresponded with the rise of many large predatory sharks (Schwimmer et al. 1997; Shimada 1997; Marmi et al. 2010; Chabain et al. 2019). Stomach content analyses have shown that stingrays are the prey of large marine predators including sharks, teleosts, and cetaceans (Gudger 1946; Randall 1967; Snelson et al. 1984; Stevens and Lyle 1989; Cliff and Dudley 1991; Lowe et al. 1996; Allen 1999; Duignan et al. 2000; National Marine Fisheries Service (NMFS) 2006). Their spines

are often found broken off and embedded in the body cavities, heads, and jaws of their predators, indicating their use as a defensive tool (Gudger 1946; Snelson et al. 1984; Cliff and Dudley 1991; Dean et al. 2017; Huskey 2021).

The spine is a two-fold defensive structure; it inflicts physical tissue damage and delivers venom to the wound. Vascular venomous tissue is housed within ventrolateral grooves along the length of the spine and covered with a protective integumentary sheath, which is ruptured during puncture and allows the venom to enter the wound (Halstead et al. 1955; Russell 1965; Enzor et al. 2011). When provoked, stingrays will elevate their tail and puncture the spine into the target or lash their tail in a side-to-side motion, which results in a slash-like laceration (Spieler et al. 2013; Hughes et al. 2018). During the strike, the spine can embed sandy, microbially rich, integument into the damaged tissue, providing additional irritation within the wound (Diaz 2008).

Advance Access publication May 14, 2021

© The Author(s) 2021. Published by Oxford University Press on behalf of the Society for Integrative and Comparative Biology. All rights reserved. For permissions please email: journals.permissions@oup.com.

The serrations located along the lateral sides of the spine are presumed to contribute to puncture and inhibit easy removal, causing further soft tissue damage (Halstead and Bunker 1953). If the spine becomes deeply embedded into the target, it will often break off or detach from the tail.

Stingrays regularly replace older primary spines with newer secondary spines. The secondary spines grow from inferior to the primary and cause it to be shed. The number of spines present varies among species. For example, the Atlantic stingray, *Hypanus sabinus*, has a maximum of two spines at any given time, (Teaf and Lewis 1987; Amesbury and Snelson 1997), whereas the spotted eagle ray, *Aetobatus narinari*, can have up to eight spines simultaneously (Gudger 1914).

Stingray spines are composed of mineralized collagen and their morphology is highly variable, both inter- and intra-specifically, in the number of serrations, serrated length of the spine, and spine cross-sectional shape (Chabain et al. 2019). Previous work has investigated the possible correlation between spine morphology and habitat among freshwater and marine species (Schwartz 2005); however, spine morphology has not been conclusively linked to ecology or phylogeny (Chabain et al. 2019). Addressing relationships between spine morphology, mineral density, and puncture and withdrawal forces will facilitate understanding of defensive puncture mechanics of the stingray spine.

For this study, we hypothesized that greater sharpness of the spine tip will result in decreased force required to puncture the target tissue, using porcine skin as a model for humans. We further hypothesized that the rear-facing serrations will catch on the punctured tissue and result in a withdrawal force that exceeds the puncture force. However, spines with a greater serration density, or pitch, have less space between each serration and it is less likely that the tissue fibers can catch on the serrations. Therefore, we hypothesized that spines with greater pitch will require lower withdrawal force. Finally, we hypothesized that the newly developed secondary spines will be less mineralized than the primary spines. To test these hypotheses, we examined two ecologically similar congeners, the Atlantic stingray, *H. sabinus* (Lesueur 1824) and the bluntnose stingray, *H. say* (Lesueur 1817). Both stingray species occur in shallow, inshore, coastal and estuarine habitats (Bigelow and Schroeder 1953; Thorson 1983; Snelson et al. 1988) and are sympatric in the Western Atlantic and Gulf of Mexico (Bigelow and Schroeder 1953; Robins and Ray 1986; Snelson et al. 1989). *Hypanus say* can grow to a larger size

(52–73 cm disc width, (Snelson et al. 1989)) than *H. sabinus* (27–45 cm disc width, (Last et al. 2016)), but they share a similar diet of gastropods, worms, and bivalves (Bigelow and Schroeder 1953; Michael 1993; Dulvy and Reynolds 1997; Smith 1997). Their overlapping ranges, similar ecologies, and congeneric relationship would lead us to hypothesize that their spine morphology and puncture/withdrawal forces should be generally similar.

Methods

Morphology

Specimens were collected during previous studies under Florida Atlantic University IACUC protocols A13-21, A16-16, A19-26, and Georgia Southern University IACUC protocol I17001. We were provided with either isolated spines or tails with spines still attached. Spines or tails were removed from wild-caught, freshly euthanized animals, and frozen before shipment; spines were never subjected to alcohol or formalin, which might have affected their mechanical properties. In the case of specimens with two spines, *primary* spines were classified as the superior spine and the newer inferior spine as *secondary* (Schwartz 2007). Only primary spines were examined morphologically and used as the puncture tool in mechanical tests. Spines were cleaned with deionized water to remove any integument and placed on a matte background with a ruler to provide a scale. The spines were photographed individually with a Nikon D70s camera equipped with a 60-mm macro lens. Photos were imported into ImageJ (Bethesda, MD), the scale was calibrated with the ruler in frame, and total spine length and serrated length were measured (cm). The number of serrations was counted from the right side of each spine (Fig. 1). Serration density, or pitch, was calculated as the number of serrations divided by the serrated length and expressed as serrations per centimeter. To quantify spine sharpness, a close-up photograph of the dorsal surface of the spine tip was taken to determine the tip included angle (Anderson 2018; Crofts and Anderson 2018). The angle tool in ImageJ was used to measure the angle formed from the margins of the left and right lateral edges of the spine tip.

Puncture testing

Puncture experiments were conducted using porcine skin as the tissue target. Adult abdominal porcine skin is often used in biomedical testing as a human model (Avon and Wood 2005; Herbig et al. 2015; Crofts and Anderson 2018) and was obtained from

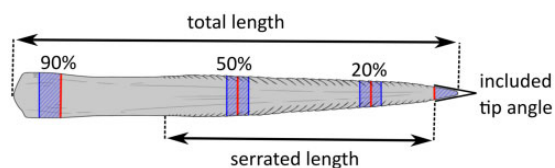


Fig. 1. Morphometrics of a representative *H. sabinus* spine. Total spine length was measured from the tip to the base, and serrated length was measured from the first serration to the last serration along the length of the spine. The tip included angle was measured from the margins of the left and right lateral edges of the spine at the tip. TMD was determined at the tip, 20, 50, and 90% (base) of the total length of the spine (vertical red lines). The TMD measurements were taken within 5% of the total length (blue shaded areas).

Sierra Medical Group (Whittier, CA; Godin and Touitou 2007; Galloway and Porter 2021). All porcine skin was shipped frozen and kept frozen until use in puncture testing; it did not undergo multiple freeze–thaw cycles. A sample of skin was thawed and dissected into squares of $\sim 2.5 \times 2.5$ cm. Skin samples were ~ 5 mm in thickness and included a 2-mm layer of skin, a 1- to 2-mm layer of underlying fat, and a 1-mm layer of muscle (Galloway and Porter 2021). A rubber dissection mat was cut into a 100×60 mm block and a well (10×10 mm, 15 mm depth) was cut into the rubber mat and filled with 5% agar. The skin was pulled taut and tightly secured with dissection pins to the rubber mat immediately above the agar well. The agar well allowed the spine to pierce completely through the skin without adding additional resistance by also piercing through the rubber mat.

Spines ($n=14$ *H. sabinus*; $n=13$ *H. say*) were secured with tension clamps to an Instron E1000 Materials Testing System outfitted with a 50 Newton (N) load cell and all mechanical tests were controlled using Bluehill Universal Software v.3.67 (Norwood, MA). The spines were clamped at 50% of total spine length and oriented with the tip facing directly downward into the porcine skin at a 90° angle. Each mechanical test consisted of three parts: puncture, 1-s hold, and withdrawal. Both puncture and withdrawal were at a rate of 30 mm min^{-1} based on previous puncture testing of a barbed spine (Crofts and Anderson 2018; Crofts et al. 2019). Slower testing speeds are often used in mechanical testing to accurately capture initial puncture forces, and/or in specific testing regimes with multiple actions such as puncture and withdrawal (Crofts and Anderson 2018; Crofts et al. 2019; Galloway and Porter 2021). Spines were driven into the skin to 20% of the total spine length to standardize among different-sized spines, and to ensure that

multiple serrations penetrated the skin. After being embedded into the skin, the spine was held in place for 1 s before starting withdrawal. The spine was withdrawn until the tip was no longer embedded into the target material. Each spine was tested only once and a new sample of skin was used for each puncture trial.

Micro-CT scanning

After puncture testing, a subset of spines ($n=11$ per species) was wrapped in gauze and scanned using micro-computed tomography (micro-CT) in a Bruker Skyscan 1173 (Kontich, Belgium). Two Bruker Skyscan-manufactured densitometry phantoms (0.25 and 0.75 g cm^{-3}) were scanned simultaneously and were used to calibrate the Skyscan CT-analyzer software (CT-An; Kontich, Belgium). The two densitometry phantoms were either wrapped with the stingray spines for scanning or were scanned separately with the same settings used to scan the spines; consistent settings (i.e., resolution and voltage) are critical for generating accurate calibrations for samples. Tissue mineral density (TMD, g cm^{-3}), the volumetric density of calcium hydroxyapatite, was calculated using Bruker DataViewer and CT-An (Kontich, Belgium) at four regions along the length of the spine: 0 (tip), 20, 50, and 90% (base) of the total length of the spine.

Analysis

All data were tested to confirm that they met the assumptions of the appropriate models before statistical testing. Data that were not normally distributed were subjected to a log transformation. If transformed data were still not normally distributed, a nonparametric test was used. To test for differences in spine morphology between species, a *t*-test or Mann–Whitney *U*-test (for nonparametric data) was applied. Linear regressions were used to investigate the relationships between the total length of the spine and morphological parameters: serration number and tip angle. A paired *t*-test was used to test for differences in puncture and withdrawal forces. A generalized linear mixed model with interaction terms was used to quantify the contribution of morphology to puncture and withdrawal forces. To evaluate mineralization among the four spine regions of fully mineralized spines, a nonparametric Friedman analysis of variance (ANOVA) with a Nemenyi post hoc test was used. All statistics were completed in R Studio 1.1.456 (<https://www.r-project.org/>) at an alpha level of 0.05.

Results

This study examined spines from 12 *H. sabinus* and 13 *H. say* specimens. Of the 12 *H. sabinus* specimens, 10 had only a single spine and 2 had two spines. For the *H. say* specimens, 12 had only a single spine and 1 had two spines. We did not include the primary *H. say* spine from the individual that had two spines due to size constraints; the primary spine was too small for the Instron tension clamps. Because we were provided with isolated spines, we lacked information on the sex or body size of the individuals and all measurements are relative to the total length of the spine.

Morphology

The mean total length of the spines did not differ significantly between species (*t*-test; $t=2.1098$, $P=0.257$) but the range of spine lengths was greater for *H. sabinus* (32.0–64.0 mm) than for *H. say* (40.2–53.1 mm). The proportion of the spine that was serrated was 50.8 ± 14.45 SD% of total spine length in *H. sabinus* and 62.3 ± 10.98 SD% in *H. say*, and this difference was significant (Mann–Whitney U-test; $Z=2.1837$, $P=0.029$).

The total number of serrations along each side of the spine was greater in *H. say* (mean = 30.4 ± 7.29 SD) compared with *H. sabinus* (mean = 20.7 ± 4.73 SD) (Mann–Whitney U test; $Z=3.2269$, $P=0.001$). The number of serrations correlated positively with spine length ($y=4.993x + 18.767$, $R^2 = 0.313$) for *H. sabinus*, and the slope was significant (ANOVA regression; $F=5.4641$, $P=0.038$) (Fig. 2). In contrast, the number of serrations correlated negatively with spine length ($y = -5.4979x + 88.189$, $R^2 = 0.024$) for *H. say*, and the low R^2 value yielded a slope that was not significant (ANOVA regression; $F=0.2682$, $P=0.615$). The pitch was 9.51 ± 2.33 SD for *H. sabinus* and 10.01 ± 1.73 SD for *H. say* and did not differ between species (*t*-test; $t=2.0639$, $P=0.534$).

Included tip angle differed between species; the tips of *H. sabinus* formed a more acute angle (mean = 16.1 ± 1.79 SD degrees) than *H. say* (mean = 19.4 ± 2.71 SD degrees) (*t*-test; $t=2.0796$, $P=0.002$). Tip angle also increased with spine length for *H. sabinus* ($y=0.3968x + 14.301$, $R^2 = 0.049$), but the low R^2 value yielded a slope that was not significant (ANOVA regression; $F=0.6249$, $P=0.448$) (Fig. 3). In contrast, tip angle decreased with spine length for *H. say* ($y = -4.9717x + 43.674$, $R^2 = 0.486$) and the slope was significant (ANOVA regression; $F=10.3809$, $P=0.008$).

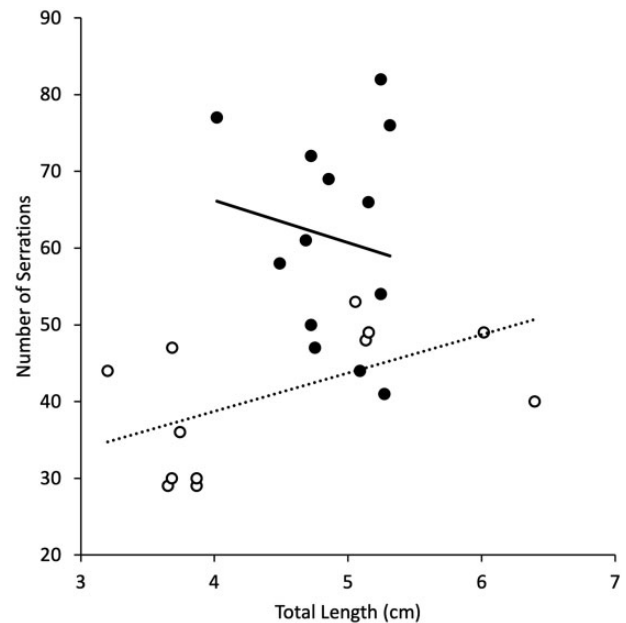


Fig. 2. Number of serrations plotted against spine length. The number of serrations was positively and significantly correlated with the total length of the spine for *H. sabinus* (open circles, dotted line). There was no significant relationship between the number of serrations and total length of the spine for *H. say* (filled circles, solid line).

Puncture testing

The mean force required to puncture into porcine skin was 3.5 ± 1.80 SD N for *H. sabinus* and 3.7 ± 3.89 SD N for *H. say* and this difference was not significant ($t=2.1199$, $P=0.269$). The mean withdrawal forces were 6.7 ± 2.98 SD N for *H. sabinus* and 5.1 ± 4.19 SD N for *H. say* and this difference was also not significant ($t=2.0796$, $P=0.092$). The mean puncture and withdrawal forces did not differ significantly for *H. say* (paired *t*-test; $t=2.0859$, $P=0.126$), but withdrawal force was significantly greater than puncture force for *H. sabinus* (paired *t*-test; $t=2.0556$, $P=0.002$). The mean puncture and withdrawal forces were significantly positively correlated for *H. say* and close to isometric ($y=0.9256x + 1.679$, $R^2 = 0.7364$, $F=30.7232$, $P<0.001$) (Fig. 4). In contrast, there was no significant relationship between puncture and withdrawal forces for *H. sabinus* due to the low R^2 value ($y=0.2097x + 5.933$, $R^2 = 0.016$, $F=0.1950$, $P=0.667$).

A generalized linear mixed model with interaction terms was used to quantify the contribution of morphology to puncture and withdrawal forces. None of the morphological variables from the generalized linear mixed model had significant interaction terms with puncture or withdrawal force for either species (Table 1).

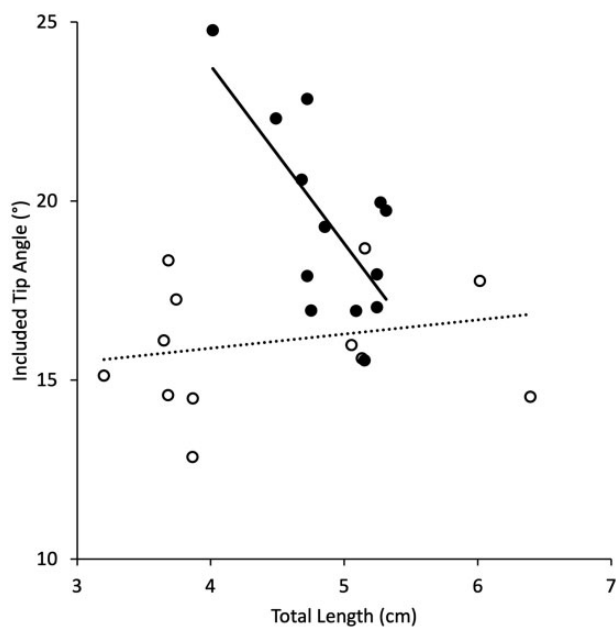


Fig. 3. Included tip angle plotted against spine total length. There was no significant relationship between included tip angle and total length of the spine for *H. sabinus* (open circles, dotted line). The included tip angle was negatively and significantly correlated with the total length of the spine for *H. say* (filled circles, solid line).

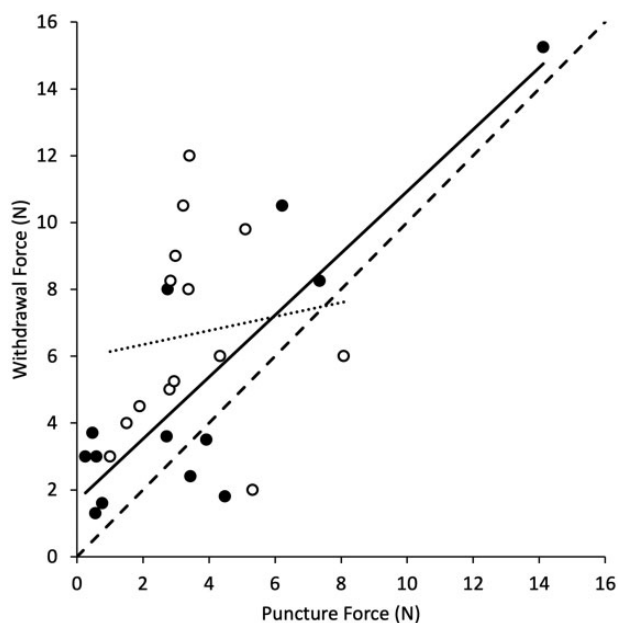


Fig. 4. Puncture and withdrawal forces of spines from *H. sabinus* (open circles, dotted line) and *H. say* (filled circles, solid line) embedded into porcine skin. Puncture and withdrawal forces are positively correlated for both species but the regression is significant only for *H. say*. The line of isometry in which puncture force equals withdrawal force is indicated by a dashed line.

Micro-CT scanning

Spine mineralization was quantified at four locations along the length of the spine; 0 (tip), 20, 50, 90% (base). Mineralization results were bimodally distributed with spines separating into either a high ($n=16$) or low ($n=6$) mineralization category. We hypothesized that the less mineralized spines were newer secondary spines from individuals that had already lost the primary spine. These less mineralized secondary spines were not included in the statistical analyses. Mineralization differed along the length of the spine for both species (Friedman ANOVA; *H. sabinus*, $Q=16.000$, $P=0.001$; *H. say*, $Q=21.480$, $P<0.001$) (Fig. 5). A Nemenyi post hoc test determined which locations were more mineralized: for both species, the 20% and 50% locations were significantly more mineralized than the base (*H. sabinus*, 20% $P=0.039$, 50% $P=0.002$; *H. say*, 20% $P=0.002$, 50% $P=0.001$). In addition, the 50% location was significantly more mineralized than the tip for both species (*H. sabinus*, $P=0.039$; *H. say*, $P=0.049$).

Discussion

Every year thousands of people worldwide are punctured by stingray spines (O'Neil et al. 2007; Diaz 2008). As humans increasingly use nearshore marine environments, stingray-human encounters will likely increase (Lowe et al. 2007). By investigating stingray spine puncture performance, we will be able to gain a better understanding of this defensive tool and possibly develop effective mitigation strategies.

Morphology and puncture performance

We hypothesized that greater spine sharpness would result in a decreased puncture force and we quantified included tip angle as a metric for sharpness. The mean included tip angle was only about 3° smaller for *H. sabinus*, and the puncture force did not differ compared with *H. say*. The radius of curvature would be an alternative to included tip angle as a metric for sharpness; however, the photographs were not taken at a sufficient magnification to capture the detail needed to confidently quantify the radius of curvature.

Previous research suggested that the recurved serrations along the length of the spine would also contribute to reducing the puncture force (Abler 1992; Cho et al. 2012; Anderson et al. 2016; Crofts and Anderson 2018). Serrations act as stress concentrators to stretch muscle fibers and facilitate the cutting of tissue, and thus reduce the force required to penetrate, as seen in barbed cactus spines and porcupine

Table 1 Results from generalized linear mixed model with interaction terms

Coefficients	t-value	P-value	Coefficients	t-value	P-value
Total length	0.424	0.674	Total length ^a	0.928	0.359
Serrated length	0.011	0.991	Test Type		
Serrations along one side	0.276	0.784	Serrated length ^a	-0.332	0.742
Included tip angle	0.382	0.704	Test Type		
Serration density	0.229	0.820	Serrations along one side ^a	0.235	0.816
Species	0.115	0.909	Test Type		
Serrations in total	-0.719	0.477	Included tip angle ^a	0.026	0.979
Test type	0.442	0.661	Test Type		
			Serration density ^a	-0.125	0.901
			Test Type		
			Species ^a	-0.572	0.571
			Test Type		
			Serrations in total ^a	-0.014	0.989
			Test Type		

There were no significant interactions between the test type (puncture and withdraw) and any of the morphological characteristics measured. Interactions between coefficients.

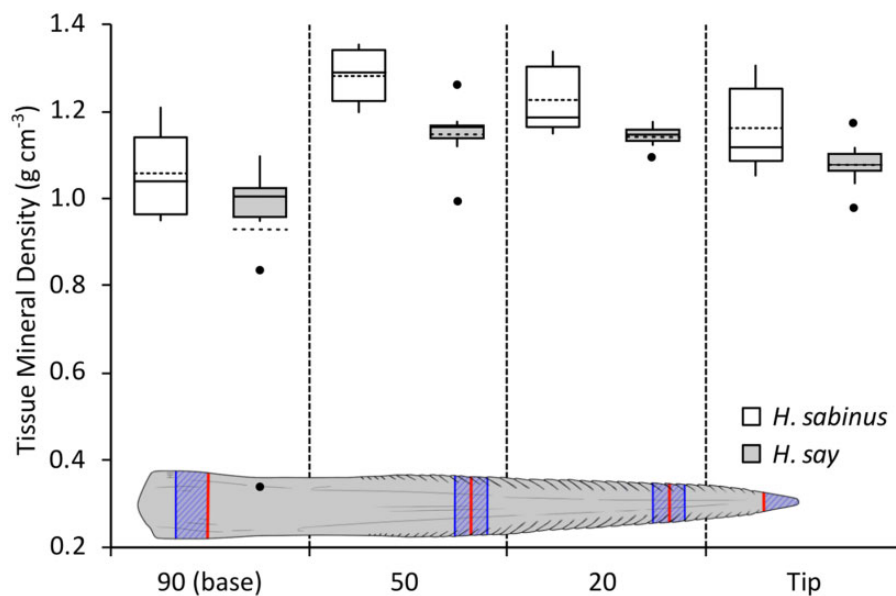


Fig. 5. Spine Tissue Mineral Density. TMD was determined along the tip, 20%, 50%, and 90% (base) of the total length of the spine. The TMD results are depicted for *H. sabinus* (open bars) and *H. say* (filled bars). The horizontal black line represents the median value and is bounded by a box at the first and third quartiles. Outliers are shown as filled circles and the mean is the horizontal dashed line. The base was less mineralized than the 20% and 50% locations, and the tip was less mineralized than the 50% location for both species.

quills (Cho et al. 2012; Crofts and Anderson 2018). The greater number of serrations in *H. say*, distributed over a greater serrated length of the spine, resulted in a pitch that did not differ from *H. sabinus*. The similar pitch of the two species yielded similar puncture forces, although the relationship might not be causal. (Anderson 2009).

We further hypothesized that the rearward-facing serrations would act as hooks that catch on the porcine skin and result in a withdrawal force greater than the puncture force. If that were the case, the slope of the regression would be greater than the line of isometry (Fig. 4). The withdrawal force scaled

nearly isometrically with the puncture force for *H. say* and the slope was less than isometric for *H. sabinus*, but the low R^2 value for *H. sabinus* does not instill confidence in the relationship. When the obvious outlier points well below the line of isometry are removed, the R^2 value increases and the slope for *H. sabinus* is more aligned with the prediction.

An additional consideration is that the rigid serrations on stingray spines do not change their orientation during withdrawal, in contrast to the barbs on cactus spines and porcupine quills that splay away from the shaft and effectively increase the size of the biological projection as it is withdrawn (Cho

et al. 2012; Crofts and Anderson 2018). As a result, the width of the puncture wound from the stingray spine is the same as that required to withdraw the spine. In these experiments, the taut skin did not fully collapse back onto the serrations, thus minimizing their effectiveness. In addition, in this controlled study, the spine was withdrawn directly through the same path as it was punctured into the target tissue. In nature, the spine and target tissue will move with respect to each other between puncture and withdrawal, so that the spine serrations will have a greater opportunity to catch on the tissue and inflict damage (Spieler et al. 2013; Hughes et al. 2018). Despite these considerations, during the puncture and withdrawal trials, stingray spine serrations did embed into the somewhat elastic skin and catch on connective tissue (Fig. 6).

This study examined puncture mechanics only in isolated mammalian skin. In reality, the skin typically overlays striated muscle. As a serrated spine is punctured through the skin and embedded into the muscle, the myofibrils pushed aside during puncture will collapse around the spine and be more readily caught on the serrations, likely resulting in a greater withdrawal force. The absence of a greater withdrawal force in these experiments is likely attributable to the taut skin being cut by the spine, and not collapsing around it during withdrawal. Future experiments could test muscle tissue in isolation, then the skin and muscle composite in situ to provide a more biologically relevant result. In addition to the puncture mechanics of target tissues, it would also be informative to measure the force required to pull a spine off of the tail, since stingrays can lose spines during defensive interactions (Cliff and Dudley 1991; Dean et al. 2017).

In this study, we used porcine skin as a model for human skin, primarily to investigate the effects of tissue damage to humans. However, the stingray spine has evolved as a defensive structure against a wide variety of predators, and it would be informative to test the puncture mechanics in different target materials, such as skin from the buccal cavity of sharks or from other large teleosts known to be batoid predators. The depth and force of puncture depend highly on the material properties of the target tissue (Anderson et al. 2016; Anderson 2018). Recent work found that shark skin with greater denticle densities may be harder to puncture than those samples or species with fewer denticles (Galloway and Porter 2021). Future work could elucidate the efficacy of the stingray spine on its intended target tissues.

We hypothesized that the pitch (serration number/serrated length of spine) could also influence puncture and withdrawal forces. We expected that spines with a greater pitch would have less space between each serration and therefore it would be less likely that the tissue fibers would catch on the serrations. In contrast, a spine with low serration density could potentially require an increased withdrawal force because of the tissue becoming more easily caught on the serrations. Other morphological characteristics not quantified here, such as fineness ratio, or serration angle, may also contribute to puncture and withdrawal forces. A spine with a low fineness ratio would have a greater width that would increase drag and result in a greater force required to puncture. Smaller serration angles would result in the serrations lying close to the shaft of the spine, whereas larger angles would orient the serrations more orthogonal to the shaft. Spines with small serration angles should have similar puncture and withdrawal forces. However, if the spine possessed large serration angles, they would increase the frontal surface area which would require greater puncture force and the orthogonal serrations would also catch more easily on the target tissue during withdrawal and thus increase the withdrawal force. Future work could fabricate 3D printed spines that span a range of morphologies to test how the shape and number of serrations affect puncture and withdrawal mechanics. This would elucidate underlying principles and tradeoffs in stingray spine design to minimize penetration force and maximize damage to the target tissue.

Differences in the position of the spine along the length of the stingray tail may also contribute to the overall puncture mechanics. The two species in this study (family Dasyatidae), possess spines located approximately midway along the length of a thin, whip-like tail. Some species, such as members of the family Urotrygonidae, have the spine located near the distal tip of a thick, muscular tail (Johansson et al. 2004; Hughes et al. 2018). Other species within the family Myliobatidae exhibit a more pelagic lifestyle and have spines located near the base of the tail that may limit the range of motion and potential effectiveness of the strike. These differences in tail morphology could produce different strike forces and kinematics.

Mineralization

We used TMD to quantify the extent of mineralization along the length of the spine and found that mineralization was not uniform along the spine

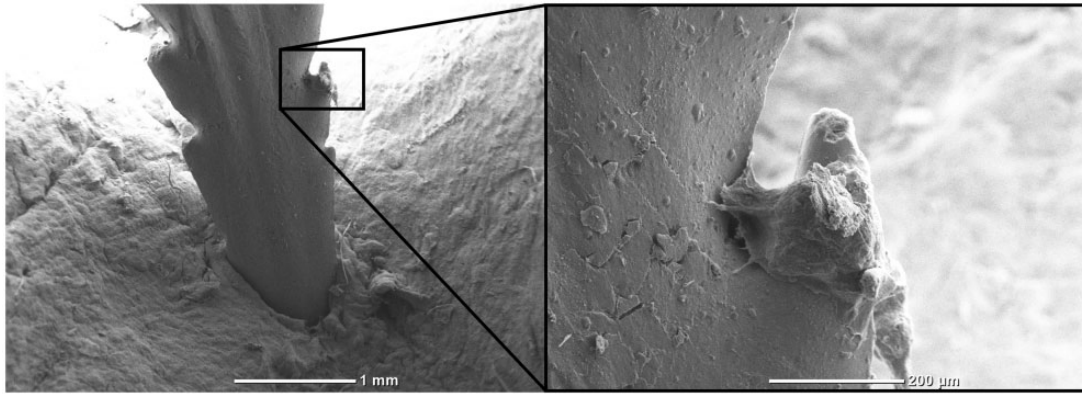


Fig. 6. Scanning electron micrograph of *H. sabinus* spine tip embedded into 5 mm thick porcine skin during puncture trials. Inset shows porcine skin tissue that remains on serrations after withdrawal. To obtain this image, porcine skin was placed in 70% ethanol and graded up to 100% ethanol before drying in a Leica EM CPD300 critical point dryer. The image was captured with a JEOL NeoScope JCM-7000 benchtop scanning electron microscope.

length. Stingray spines can be considered highly mineralized; TMD measurements from both species at 20% and 50% of spine locations fall at the greater end of the range for mineral density calculations from human femur cortical bone ($0.54\text{--}1.35\text{ g cm}^{-3}$; Lang et al. 2004). Greater mineralization confers greater material strength (ability to resist failure) and stiffness (rigidity). However, hypermineralization correlates the most strongly with stiffness, which can render a material less tough (ability to absorb energy); a stiff material is more brittle and may break more easily (Turner 2002; Vogel 2003). If stingray spines are most brittle in the middle of the shaft, then the spine could fracture at this location after it was impaled into a predator. A brittle spine shaft could allow the stingray to escape after inflicting damage to a predator and thus minimize the risk of tissue damage to its own body.

We found that TMD was bimodally distributed, with most spines exhibiting a high level of mineralization, whereas some were much less mineralized. We hypothesized that the more mineralized spines were the older, primary spines and the less mineralized spines were the newer, secondary spines that were growing in to replace the primary spine, but had not yet fully mineralized. Spines were only identified as primary or secondary when two spines were present on an individual. Most individuals possessed only a single spine, which was classified as the primary. It is possible that some of the spines classified as primary (on individuals with only one spine) could actually have been secondary spines, and the primary spine had been shed or fallen off recently prior to the animal being caught. This could account for the low TMD values of some of the spines in our study. To overcome this potentially confounding

factor, the analyses here were conducted on only one mode from the TMD results: the more mineralized spines. If secondary spines are less mineralized than primaries, then we expect that they will be less brittle and less likely to break during puncture and withdrawal. Additionally, individual stingrays could have potentially suffered from pathology or injury that compromised body tissues, including mineral deposits in their defensive structures. The present study collected samples from deceased wildlife whose life histories are unknown; this introduces a limitation regarding the extent that we can account for confounding factors compared with studies that test TMD in model systems such as mice. Future studies could test whether primary and secondary spines differ in TMD and brittleness by sampling captive specimens between May and August, when *H. sabinus* is known to have two spines prior to shedding the primary spine (Teaf and Lewis 1987; Amesbury and Snelson 1997).

Future directions

This study compared the spines from two ecologically similar congeners, although the spines of *H. say* represented a smaller range of sizes than the spines from *H. sabinus*. The largest spine of *H. say* was $\sim 32\%$ longer than the smallest spine, whereas in *H. sabinus*, the longest spine was double the length of the smallest. We also observed a high degree of variation in spine morphometrics from both species. This variation, coupled with the small range of spine lengths for *H. say*, might have obscured some relationships and differences between the species. A larger sample size, that included spines from a full ontogenetic series, would help to illuminate potential differences between species. Additionally, testing

species from across a wider ecological and phylogenetic range would inform us about morphology, mineralization, mechanical performance, and the efficacy of different spine shapes. More to the point, this article takes a first stab at examining the puncture mechanics of stingray spines, and future studies should examine a wide range of species, animal sizes, and ecologically relevant target materials.

Acknowledgments

We thank C. Bedore, M. Ajemian, M. McCallister, and the members of the Florida Atlantic University—Harbor Branch Oceanographic Institute Fisheries Ecology and Conservation Lab for supplying some of the specimens; M. Smith for assistance with all aspects of the laboratory work; T. Meredith and the Florida Atlantic University Owls Imaging Lab for access to the micro-CT scanner; K. Wallace for Instron support; and I. Heerdegen for preparation of the spine illustration in Fig. 1.

Data availability

The data underlying this article will be shared on reasonable request to the corresponding author.

References

- Abler WL. 1992. The serrated teeth of tyrannosaurid dinosaurs, and biting structures in other animals. *Paleobiology* 18:161–83.
- Allen TB. 1999. *The shark almanac*. New York, NY: The Lyons Press.
- Amesbury E, Snelson FF. 1997. Spine replacement in a freshwater population of Atlantic stingray, *Dasyatis sabina*. *Copeia* 1997:220–3.
- Anderson PSL. 2009. The effects of trapping and blade angle of notched dentitions on fracture of biological tissues. *J Exp Biol* 212:3627–32.
- Anderson PSL. 2018. Making a point: shared mechanics underlying the diversity of biological puncture. *J Exp Biol* 221:jeb187294.
- Anderson PSL, LaCosse J, Pankow M. 2016. Point of impact: the effect of size and speed on puncture mechanics. *Interf Focus* 6:20150111.
- Avon S, Wood R. 2005. Porcine skin as an porcine skin as an in-vivo model for model for ageing of human bite marks. *J Forensic Odontostomatol* 23:30–9.
- Bigelow HB, Schroeder WC. 1953. *Fishes of the western North Atlantic*. Part 2. Sawfishes, guitarfishes, skates, rays, and chimaeroids. New Haven, CT: Memoirs Sears Foundation for Marine Research, Yale University.
- Chabain JJ, Summers AP, Kolmann MA. 2019. What's the point?: Form and function of the caudal barb in stingrays (Talk), Society for Integrative and Comparative 2019 Annual Meeting, January 4–6 in Tampa, FL.
- Cho WK, Ankrum J, Guo D, Chester SA, Yang SY, Kashyap A, Campbell GA, Wood RJ, Rijal RK, Karnik R, et al. 2012. Microstructured barbs on the North American porcupine quill enable easy tissue penetration and difficult removal. *Proc Natl Acad Sci U S A* 109:21289–94.
- Cliff G, Dudley SFJ. 1991. Sharks caught in the protective gill nets of Natal, South Africa. 4: the Bull shark *Carcharhinus leucas* Valenciennes. *Afr J Mar Sci* 10:253–70.
- Crofts SB, Anderson PSL. 2018. The influence of cactus spine surface structure on puncture performance and anchoring ability is tuned for ecology. *Proc R Soc B* 285:2018–280.
- Crofts SB, Lai Y, Hu Y, Anderson PSL. 2019. How do morphological sharpness measures relate to puncture performance in viperid snake fangs? *Biol Lett* 15:20180905. <https://doi.org/10.1098/rsbl.2018.0905>
- Dean MN, Bizzarro JJ, Clark B, Underwood CJ, Johanson Z. 2017. Large batoid fishes frequently consume stingrays despite skeletal damage. *R Soc Open Sci* 4:170674.
- Diaz J. 2008. The evaluation, management, and prevention of stingray injuries in travelers. *J Travel Med* 15:102–9.
- Duignan PJ, Hunter JEB, Visser IN, Jones GW, Nutman A. 2000. Stingray spines: a potential cause of killer whale mortality in New Zealand. *Aquat Mamm* 26:143–7.
- Dulvy NK, Reynolds JD. 1997. Evolutionary transitions among egg-laying, live-bearing and maternal inputs in sharks and rays. *Proc R Soc Lond Ser B: Biol Sci* 264:1309–15.
- Enzor LA, Wilborn RE, Bennett WA. 2011. Toxicity and metabolic costs of the Atlantic stingray (*Dasyatis sabina*) venom delivery system in relation to its role in life history. *J Exp Mar Biol Ecol* 409:235–9.
- Galloway KA, Porter ME. 2021. Predator–prey interactions examined using lionfish spine puncture performance. *IOB* 2021:3.
- Godin B, Touitou E. 2007. Transdermal skin delivery: predictions for humans from in vivo, ex vivo and animal models. *Adv Drug Deliv Rev* 59:1152–61.
- Gudger EW. 1914. History of the spotted eagle ray, *Aetobatus narinari*, together with a study of its external structures. Chapter XII. In: *Papers from the Tortugas Laboratory of the Carnegie Institution of Washington*. Vol. XI. Washington, DC: Carnegie Institute Washington, p. 248–323.
- Gudger EW. 1946. Does the stingray strike and poison fishes? *Sci Mon* 63:110–6.
- Halstead BW, Bunker N. 1953. Stingray attacks and their treatment. *Am J Trop Med Hyg* 2:115–28.
- Halstead BW, Ocampo RR, Modglin FR. 1955. A study on the comparative anatomy of the venom apparatus of certain North American stingrays. *J Morphol* 97:1–21.
- Herbig ME, Houdek P, Gorissen S, Zorn-Kruppa M, Wladykowski E, Volksdorf T, Grzybowski S, Kolios G, Willers C, Mallwitz H, et al. 2015. A custom tailored model to investigate skin penetration in porcine skin and its comparison with human skin. *Eur J Pharm Biopharm* 95:99–109.
- Hughes R, Pedersen K, Huskey S. 2018. The kinematics of envenomation by the yellow stingray, *Urobatris jamaicensis*. *Zoomorph* 137:409–18.
- Huskey S. 2021. Stingray spines embedded in the skull of a cobia. *Ichthyol Res* 68:214–6.

- Johansson PKE, Douglass TG, Lowe CG. 2004. Caudal spine replacement and histogenesis in the round stingray, *Urobatis halleri*. *Bull South Cali Acad Sci* 103:115–24.
- Lang T, LeBlanc A, Evans H, Lu Y, Genant H, Yu A. 2004. Cortical and trabecular bone mineral loss from the spine and hip in long-duration spaceflight. *J Bone Miner Res* 19:1006–12.
- Last PR, White WT, de Carvalho MR, Séret B, Stehmann MFW, Naylor GJP. 2016. *Rays of the world*. Ithaca: CSIRO Publishing, Comstock Publishing Associates.
- Lesueur CA. 1817. Description of three new species of the genus *Raja*. *J Acad Nat Sci Phila* 1:41–5.
- Lesueur CA. 1824. Description of several species of the Linnaean genus *Raia*, of North America. *J Acad Nat Sci Phila* 4:100–21.
- Lowe CG, Moss GJ, Hoisington GIV, Vaudo JJ, Cartamil DP, Marcotte MM, Papastamatiou YP. 2007. Caudal spine shedding periodicity and site fidelity of round stingrays, *Urobatis halleri* (Cooper), at Seal Beach, California: implications for stingray-related injury management. *Bull South Calif Acad Sci* 106:16–26. –
- Lowe CG, Wetherbee BM, Crow GL, Tester AL. 1996. Ontogenetic dietary shifts and feeding behavior of the tiger shark, *Galeocerdo cuvier*, in Hawaiian waters. *Environ Bio Fishes* 47:203–11.
- Marmi J, Vila B, Oms O, Galobart A, Cappetta H. 2010. Oldest records of stingray spines (Chondrichthyes, Myliobatiformes). *J Vertebr Paleontol* 30:970–4.
- Michael SW. 1993. *Reef sharks and rays of the world: a guide to their identification, behavior, and ecology*. Monterey, CA: Sea Challengers.
- National Marine Fisheries Service (NMFS). 2006. Status report on the continental United States distinct population segment of the goliath grouper (*Epinephelus itajara*). St. Petersburg, FL: National Marine Fisheries Service (NMFS).
- O’Neil ME, Mack KA, Gilchrist J. 2007. Epidemiology of non-canine bite and sting injuries treated in U.S. emergency departments, 2001–2004. *Public Health Rep* 122:764–75.
- Randall JE. 1967. Food habits of reef fishes of the West Indies. *Stud Trop Oceanogr* 5:665–847.
- Robins CR, Ray GC. 1986. *A field guide to Atlantic coast fishes*. Boston, MA: Houghton Mifflin.
- Russell FE. 1965. Marine toxins and venomous and poisonous marine animals. *Adv Mar Biol* 3:255–384.
- Schwartz F. 2005. Tail spine characteristics of stingrays (Order Myliobatiformes) found in the northeast Atlantic, Mediterranean, and Black Seas. *Electron J Ichthyol* 1:1–9.
- Schwartz F. 2007. A survey of tail spine characteristics of stingrays frequenting African, Arabian to Chagos-Maldives Archipelago waters. *Smithiana Bulletin* 8:41–52.
- Schwimmer DR, Stewart JD, Williams GD. 1997. Scavenging by sharks of the genus *Squalicorax* in the Late Cretaceous of North America. *Palaios* 12:71–83.
- Shimada K. 1997. Paleocological relationships of the Late Cretaceous lamniform shark, *Creotoxryhina mantelli* (Agassiz). *J Paleontol* 71:926–33.
- Smith CL. 1997. National Audubon Society field guide to tropical marine fishes of the Caribbean, the Gulf of Mexico, Florida, the Bahamas, and Bermuda. New York, NY: Alfred A. Knopf, Inc.
- Snelson FF Jr, Mulligan TJ, Williams SE. 1984. Food habits, occurrence, and population structure of the bull shark, *Carcharhinus leucas*, in Florida coastal lagoons. *Bull Mar Sci* 34:71–80.
- Snelson FF Jr., Williams-Hooper SE, Schmid TH. 1988. Reproduction and ecology of the Atlantic stingray, *Dasyatis sabina*, in Florida coastal lagoons. *Copeia* 1988:729–39.
- Snelson FF Jr., Williams-Hooper SE, Schmid TH. 1989. Biology of the bluntnose stingray, *Dasyatis sayi*, in Florida coastal lagoons. *Bull Mar Sci* 45:15–25.
- Spieler RE, Fahy DP, Sherman RL, Sulikowski J, Quinn TP. 2013. The yellow stingray, *Urobatis jamaicensis* (Chondrichthyes Urotrygonidae): a synoptic review. *Carib J Sci* 47:67–97.
- Stevens JD, Lyle JM. 1989. Biology of three hammerhead sharks (*Eusphyra blochii*, *Sphyrna mokarran* and *S. lewini*) from Northern Australia. *Aus J Mar Fresh Res* 40:129–46.
- Su FY, Bushong EA, Deerinck TJ, Seo K, Herrera S, Graeve OA, Kisailus D, Lubarda VA, McKittrick J. 2017. Spines of the porcupine fish: structure, composition, and mechanical properties. *J Mech Behav Biomed* 73:38–49.
- Teaf CM, Lewis TC. 1987. Seasonal occurrence of multiple caudal spines in the Atlantic Stingray, *Dasyatis sabina* (Pisces: dasyatidae). *Copeia* 1:224–7.
- Thorson TB. 1983. Observations on the morphology, ecology, and life history of the euryhaline stingray, *Dasyatis guttata* (Bloch and Schneider) 1801. *Acta Biol Venez* 11:95–125.
- Turner CH. 2002. Biomechanics of bone: determinants of skeletal fragility and bone quality. *Osteoporos Int* 13:97–104.
- Vogel S. 2003. *Comparative biomechanics: life’s physical world*. Princeton, NJ: Princeton University Press.